



OPEN

## Design and synthesis of $\text{Fe}_3\text{O}_4@ \text{SiO}_2@ \text{KIT-6}@ \text{DTZ-Pd}^0$ as a new and efficient mesoporous magnetic catalyst in carbon–carbon cross-coupling reactions

Zahra Moradi<sup>1</sup> & Arash Ghorbani-Choghamarani<sup>2</sup>✉

In this paper, a new type of mesoporous material based on KIT-6 has been introduced. In this aim, magnetic  $\text{Fe}_3\text{O}_4$  nanoparticles and mesoporous silica KIT-6 have been combined to obtain mesoporous MNPs. The prepared magnetic mesoporous catalyst has been applied in different carbon–carbon cross-coupling reactions including Mizoroki–Heck, Suzuki–Miyaura, and Stille reactions. This magnetic mesoporous compound is characterized by various techniques including FT-IR, BET, VSM, SEM, XRD, and TGA.

Mesoporous materials are solid and porous compounds with nanometer pore sizes and very high available surfaces area. These porous materials are made of two parts: cavities and walls. In the last few years, a different category of porous materials has been recognized and introduced to chemistry science, such as silica structures, metal oxides, silicon nanopores, carbon nanotubes, and porous carbon. The regular and porous silica structures were discovered in the 1990s<sup>1–3</sup>. High specific level, selectivity, shape, and size are the most significant characteristics of these materials, which convert them to critical materials with a wide range of applications such as catalysis, filtration and isolation etc.<sup>4,5</sup>. Major applications of nanopores in chemistry are their use in the manufacture of chemical sensors and application as a surface for the stabilization of chemical and biochemical catalysts. The development of these materials in the future depends on the manufacture of engineered and controlled porosity for the given applications<sup>6–10</sup>. Based on the size of the channel diameters, nanoporous materials are divided into three main categories: macroporous, mesoporous and microporous. The most important members of mesoporous, which are named as M41S family, include MCM-41, MCM-48, and MCM-50 mesopores<sup>11,12</sup>.

The KIT-6 structure is a relatively new structure of mesoporous silica, which has first been synthesized by Rio et al. in 2003 that has a cubic bilateral structure of  $Ia_3d$  symmetry and cylindrical cavities and the advantage of this structure compared to other silica structures is the higher cavities volumes<sup>13,14</sup>. This three-dimensional silica grid can be a suitable host for various components, which can easily enter the cavity and spread out. KIT-6 has been recognized with wide applications including electrical, catalytic, and isolation applications<sup>15–18</sup>.

One of the most important chemists' achievements is the discovery of the carbon–carbon coupling reactions in the presence of a complex containing transition metal such as copper, palladium, nickel, and iron. Among transition metals complexes, palladium is one of the best choices, due to its simple complex preparation, high activity, and selectivity in coupling reactions<sup>19–24</sup>. In organic chemistry science, a variety of coupling reaction systems has been discovered, designed, and introduced: Heck reaction<sup>25</sup>, Suzuki reaction<sup>26</sup>, Negishi reaction<sup>27</sup>, Stille reaction<sup>28</sup>, Sonogashira reaction<sup>25</sup>, Kumada coupling<sup>26</sup>, Hiyama coupling reaction<sup>27</sup>, and Buchwald–Hartwig reaction<sup>29</sup>. Among them, Stille (coupling reaction of a tin organic compound with an electro-friendly organic compound)<sup>30</sup>, Suzuki (coupling reaction of a phenylboronic acid derivative with various aryl halides)<sup>31</sup>, and Heck reaction (coupling reaction of aryl of various halides with alkenes)<sup>32</sup> are main and generally applicable methods for the construction of carbon–carbon bonds<sup>33,34</sup>. Herein we have synthesized a new immobilized palladium complex on the modified magnetic mesoporous material ( $\text{Fe}_3\text{O}_4@ \text{SiO}_2@ \text{KIT-6}@ \text{DTZ-Pd}^0$ ) that acts as a versatile catalyst in cross-coupling reactions.

<sup>1</sup>Department of Chemistry, Faculty of Sciences, Ilam University, P.O. Box 69315516, Ilam, Iran. <sup>2</sup>Department of Organic Chemistry, Faculty of Chemistry, Bu-Ali Sina University, P.O. Box 6517838683, Hamedan, Iran. ✉email: a.ghorbani@ilam.ac.ir

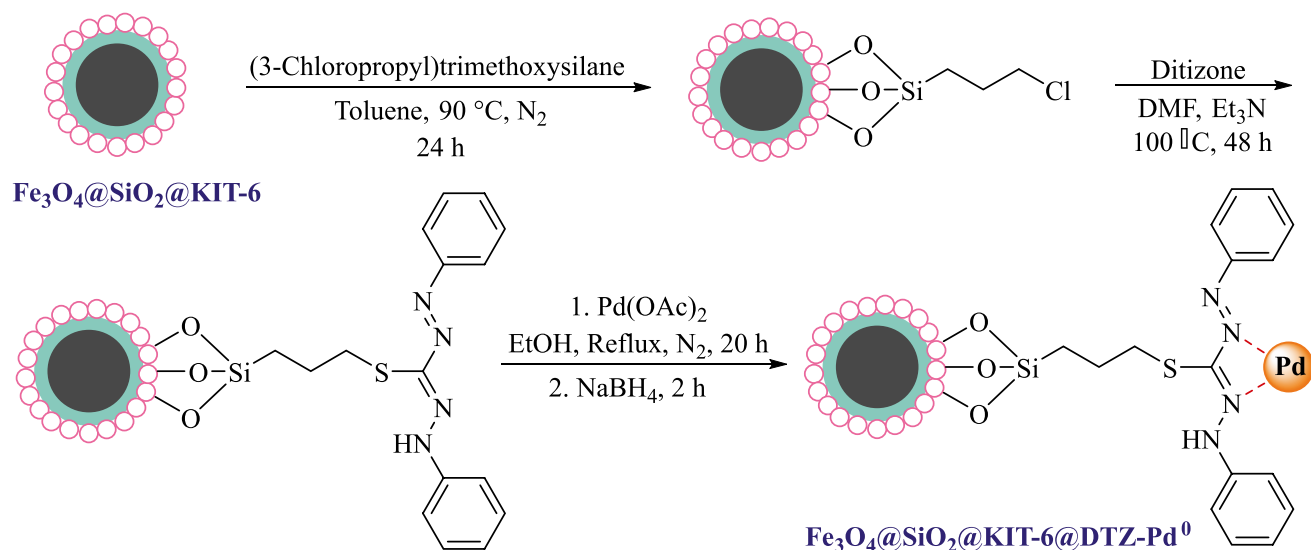


**Figure 1.** Stepwise preparation of Fe<sub>3</sub>O<sub>4</sub>@SiO<sub>2</sub>@KIT-6@DTZ-Pd<sup>0</sup>.

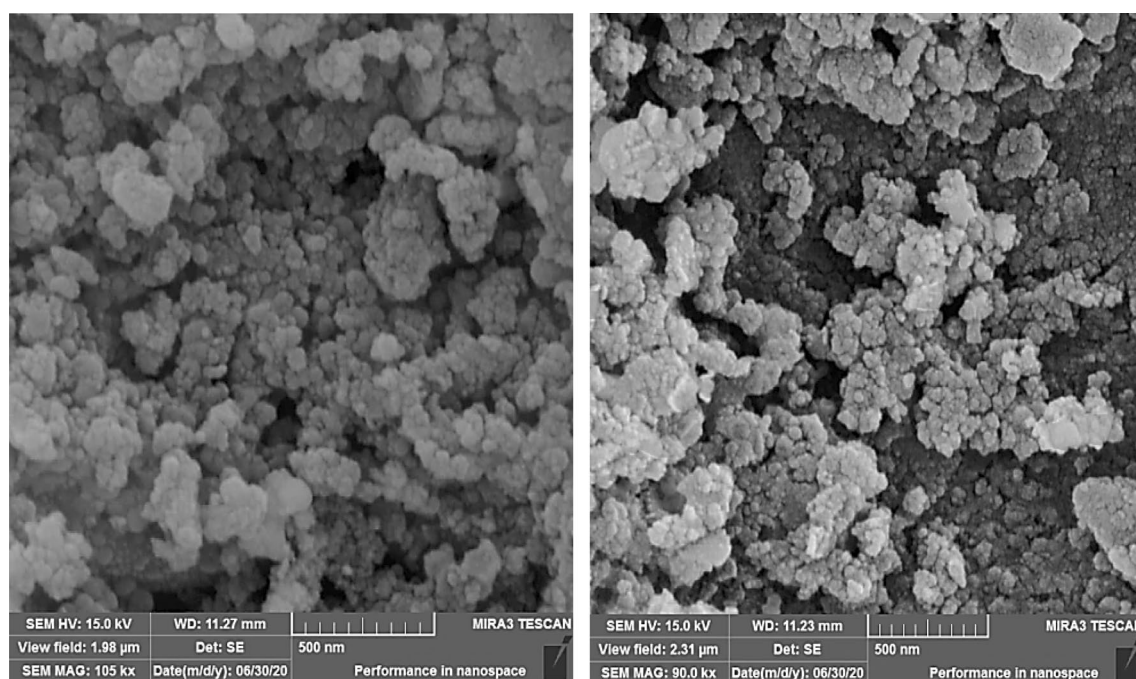


**Figure 2.** SEM images of the Fe<sub>3</sub>O<sub>4</sub>@SiO<sub>2</sub>@KIT-6@DTZ-Pd<sup>0</sup> at different magnification.

## Result and discussion

**Preparation and characterization of Fe<sub>3</sub>O<sub>4</sub>@SiO<sub>2</sub>@KIT-6@DTZ-Pd<sup>0</sup>.** For the synthesis of Fe<sub>3</sub>O<sub>4</sub>@SiO<sub>2</sub>@KIT-6@DTZ-Pd<sup>0</sup> catalyst, first Fe<sub>3</sub>O<sub>4</sub> magnetic nanoparticles were synthesized by co-precipitation method<sup>35</sup>. Subsequently, it was coated by KIT-6 to synthesize Fe<sub>3</sub>O<sub>4</sub>@SiO<sub>2</sub>@KIT-6 nanoparticles. In the next step, obtained Fe<sub>3</sub>O<sub>4</sub>@SiO<sub>2</sub>@KIT-6 modified by (3-chloropropyl) triethoxysilane. Finally, to obtain the final catalyst Fe<sub>3</sub>O<sub>4</sub>@SiO<sub>2</sub>@KIT-6-nPrNH<sub>2</sub> condensed with dithizone followed by coordination with palladium as outlined in Fig. 1.

After designing and fabricating Fe<sub>3</sub>O<sub>4</sub>@SiO<sub>2</sub>@KIT-6@DTZ-Pd<sup>0</sup>, the structure of this magnetic mesoporous material is characterized by various techniques.

To consider the morphology of prepared magnetic mesoporous material, SEM (scanning electron microscopy) was applied. As it can be seen in Fig. 2, Fe<sub>3</sub>O<sub>4</sub>@SiO<sub>2</sub>@KIT-6@DTZ-Pd<sup>0</sup> particles are spherical with nano-sized particles.

Porosity analysis of Fe<sub>3</sub>O<sub>4</sub>@SiO<sub>2</sub>@KIT-6@DTZ-Pd<sup>0</sup> studied by nitrogen absorption–desorption technique. Based on this analysis, the specific surface area of Fe<sub>3</sub>O<sub>4</sub>@SiO<sub>2</sub>@KIT-6@DTZ-Pd<sup>0</sup> (a<sub>SBET</sub>) was 71.477 m<sup>2</sup>/g, its monolayer capacity (V<sub>m</sub>) was 16.422 cm<sup>3</sup> (STP) g<sup>-1</sup> and the total pore volume of the prepared magnetic mesoporous compound was 0.1188 cm<sup>3</sup>/g. The specific surface area was calculated by the Langmuir isotherm.

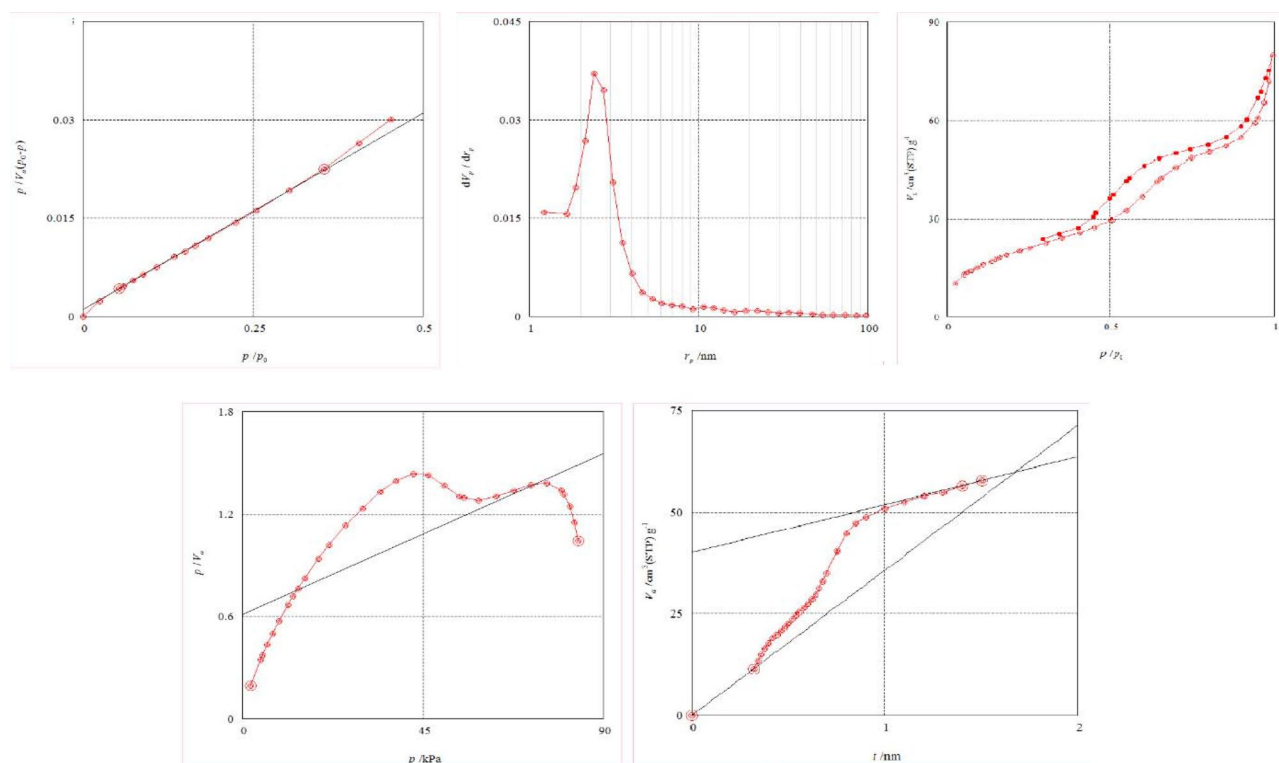


**Figure 3.**  $N_2$  adsorption–desorption isotherms of  $Fe_3O_4@SiO_2@KIT-6@DTZ-Pd^0$ .

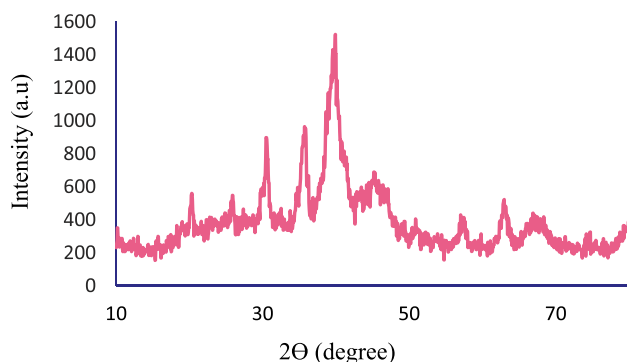


**Figure 4.** The XRD pattern of the  $Fe_3O_4@SiO_2@KIT-6@DTZ-Pd^0$ .

Langmuir isotherm (Fig. 3) illustrated  $a_{s,lang} = 415.1 \text{ m}^2/\text{g}$  and  $V_m = 95.372 \text{ cm}^3 (\text{stp}) \text{ g}^{-1}$ , respectively. Furthermore, the calculations related to BJH diagram from the adsorption and desorption branch of the nitrogen adsorption curve indicated that the pore sizes in these compounds were the same and the average pore diameter of  $Fe_3O_4@SiO_2@KIT-6@DTZ-Pd^0$  is 2.41 nm.

To measure the exact amount of loaded Pd on the surface of  $Fe_3O_4@SiO_2@KIT-6@DTZ$  nanoparticles, induced coupled plasma (ICP) spectroscopy technique was used, which based on this technique, the exact amount of Pd is  $1.069 \times 10^{-3} \text{ mol/g}$ .

The XRD pattern of  $Fe_3O_4@SiO_2@KIT-6@DTZ-Pd^0$  nanoparticles is displayed in Fig. 4. As it can be seen, the XRD pattern of synthesized nanoparticle shows characteristic peaks at  $2\theta = 25.86^\circ, 30.46^\circ, 35.71^\circ, 43.46^\circ, 53.86^\circ, 57.01^\circ, 62.86^\circ,$  and  $74.16^\circ$  that are related to  $Fe_3O_4$  and the extent peak appearing in  $2\theta$  of  $20.26^\circ$  are related to the presence of a silica layer around the nanoparticles. The corresponding peaks at  $2\theta = 39.91^\circ, 45.16^\circ$  and  $66.86^\circ$  is correspondence to Pd particles. These pieces of evidence show that Pd is well stabilized on the nanocatalyst<sup>36,37</sup>.

The TGA diagram for magnetic mesoporous material ( $Fe_3O_4@SiO_2@KIT-6@DTZ-Pd^0$ ) is shown in Fig. 5. Based on this analysis, the first weight loss under  $200^\circ\text{C}$  (about 10%) is related to the evaporation of physically adsorbed solvents and water. The second weight loss, which is about 9.5%, is between  $200$  to  $800^\circ\text{C}$  related to the removal of organic moieties on the surface of magnetic mesoporous support. The final weight loss is related to the phase change of  $Fe_3O_4@SiO_2@KIT-6@DTZ-Pd^0$  nanoparticles.

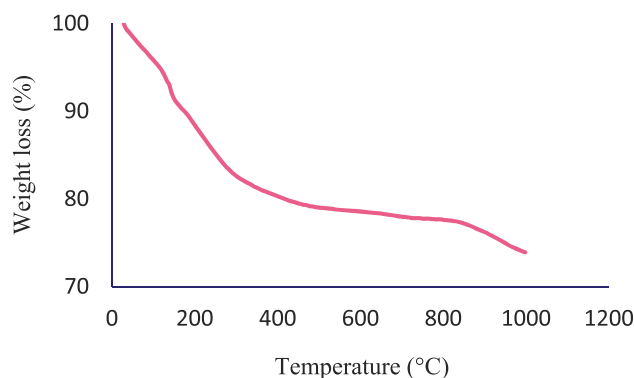


**Figure 5.** TGA thermogram of the  $\text{Fe}_3\text{O}_4@SiO_2@KIT-6@DTZ-Pd^0$ .

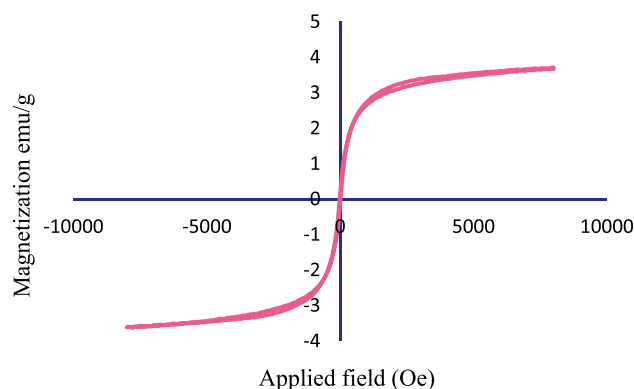


**Figure 6.** Magnetization curves for  $\text{Fe}_3\text{O}_4@SiO_2@KIT-6@DTZ-Pd^0$  at room temperature.

The magnetic properties of the synthesized  $\text{Fe}_3\text{O}_4@SiO_2@KIT-6@DTZ-Pd^0$  were investigated by VSM analysis. As displayed in Fig. 6, the magnetic property of nanocatalyst is 3.67 emu/g, which reflects this fact, the nanoparticle surface is coated with  $\text{SiO}_2$  and organic groups. Nevertheless, by applying an external magnetic field, the catalyst can be easily separated from the reaction mixture.

The FT-IR spectra of  $\text{Fe}_3\text{O}_4@SiO_2@KIT-6$  (a),  $\text{Fe}_3\text{O}_4@SiO_2@KIT-6@CPTES$  (b),  $\text{Fe}_3\text{O}_4@SiO_2@KIT-6@DTZ$  (c),  $\text{Fe}_3\text{O}_4@SiO_2@KIT-6@DTZ-Pd^0$  (d) and recovered  $\text{Fe}_3\text{O}_4@SiO_2@KIT-6@DTZ-Pd^0$  (e) are shown in Fig. 7. The FT-IR spectra of  $\text{Fe}_3\text{O}_4@SiO_2@KIT-6$  (Fig. 7a) indicated several bands at  $463\text{ cm}^{-1}$ ,  $637\text{ cm}^{-1}$ , which is related to stretching vibration of Fe–O bond, and a sharp peak at  $1079\text{ cm}^{-1}$  belong to stretching vibration of Si–O–Si bond, two peaks at  $1634\text{ cm}^{-1}$  and  $3433\text{ cm}^{-1}$  related to bending vibration and stretching vibration OH groups, respectively. Several peaks about  $2900\text{ cm}^{-1}$  are related to C–H stretching vibration and the bending vibration for Si–O–Si bond appears at  $1078\text{ cm}^{-1}$  in the IR spectra of  $\text{Fe}_3\text{O}_4@SiO_2@KIT-6@CPTES$  (Fig. 7b). In the next spectra (Fig. 7c) the observed peaks at  $3436\text{ cm}^{-1}$  and  $1650\text{ cm}^{-1}$  are related to N–H and C=N bonds, also the observed peak at  $1391\text{ cm}^{-1}$  is belongs to the stretching vibration of C=S bond. The shifting of C=N peak from  $1650$  to  $1634\text{ cm}^{-1}$  in IR spectra of  $\text{Fe}_3\text{O}_4@SiO_2@KIT-6@DTZ-Pd$  (Fig. 7d) indicating that palladium was successfully coordinated to dithizone. The FT-IR spectra of recovered  $\text{Fe}_3\text{O}_4@SiO_2@KIT-6@DTZ-Pd^0$  (Fig. 7e), after the four times recovery, do not show any significant change with the fresh catalyst.

**Catalytic studies.** *Mizoroki–Heck cross-coupling reaction.* After the characterization of the prepared magnetic mesoporous material, the catalytic activity of this compound was studied in carbon–carbon bond formation reactions.

Initially, the catalytic activity of  $\text{Fe}_3\text{O}_4@SiO_2@KIT-6@DTZ-Pd^0$  was examined in Heck reaction. To obtain optimal conditions for this C–C cross-coupling reaction, the reaction of iodobenzene and butyl acrylate was investigated as a model reaction. The reaction was examined in the presence of various solvents such as PEG, DMF, DMSO,  $\text{CH}_3\text{CN}$ , different bases (KOH, NaOH,  $\text{Na}_2\text{CO}_3$ ,  $\text{Li}_2\text{CO}_3$ ), and different values of catalysts (4, 5, and 6 mg) at various temperature conditions.

The highest yield of product (95%) was obtained in PEG as the solvent, 3 mmol of  $\text{K}_2\text{CO}_3$  as the base and 5 mg of catalyst at  $100\text{ }^\circ\text{C}$  (Table 1).

To develop the efficiency of described catalyst a variety of aryl halides reacted with butyl acrylate under obtained optimal reaction conditions (Scheme 1).

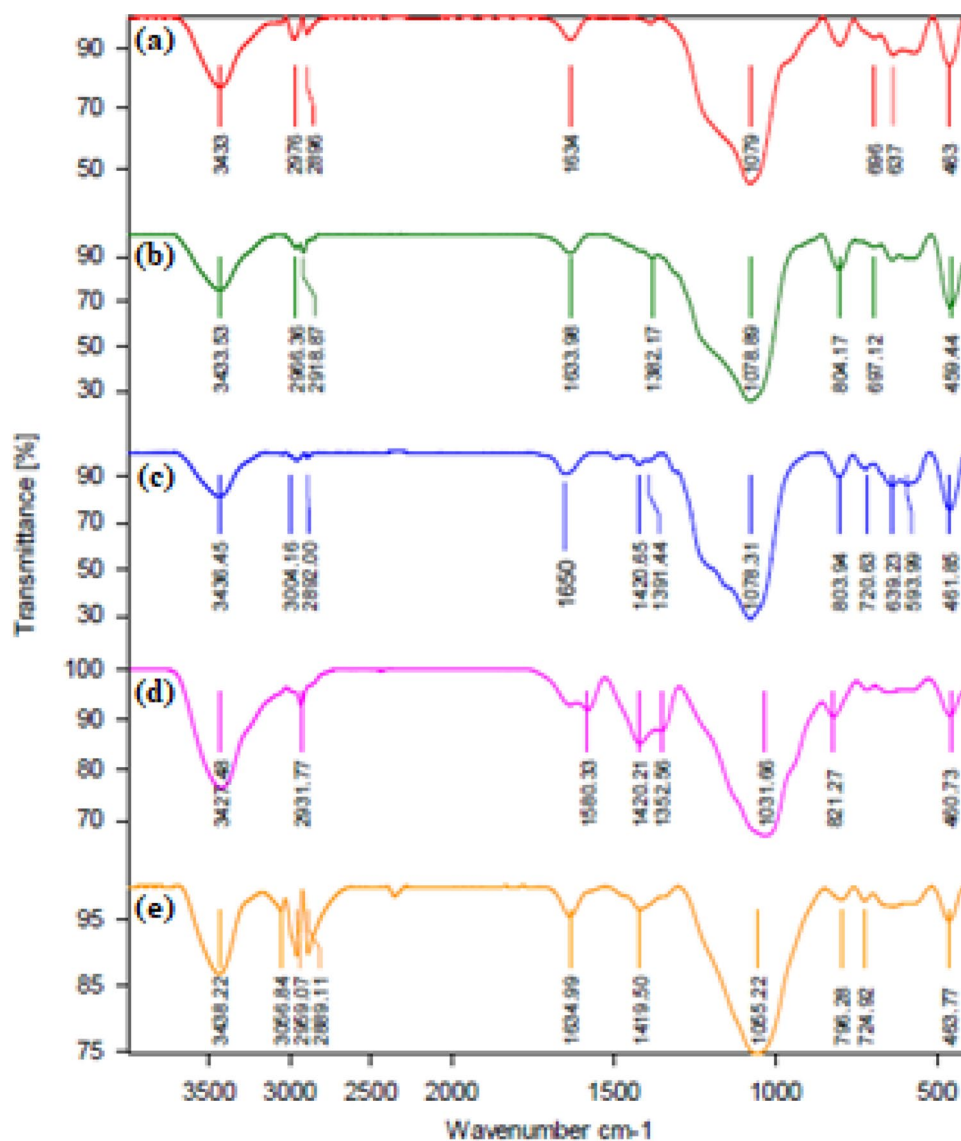


**Figure 7.** The FT-IR spectra of Fe<sub>3</sub>O<sub>4</sub>@SiO<sub>2</sub>@KIT-6 (a), Fe<sub>3</sub>O<sub>4</sub>@SiO<sub>2</sub>@KIT-6@CPTES (b), Fe<sub>3</sub>O<sub>4</sub>@SiO<sub>2</sub>@KIT-6@DTZ (c), Fe<sub>3</sub>O<sub>4</sub>@SiO<sub>2</sub>@KIT-6@DTZ-Pd<sup>0</sup> (d) and recovered Fe<sub>3</sub>O<sub>4</sub>@SiO<sub>2</sub>@KIT-6@DTZ-Pd<sup>0</sup> (e).

The results are summarized in Table 2. As it can be seen, aryl iodides are not significantly different from aryl bromides and chlorides in terms of the reaction yields, and only the reaction time with aryl bromides and aryl chlorides is slightly longer.

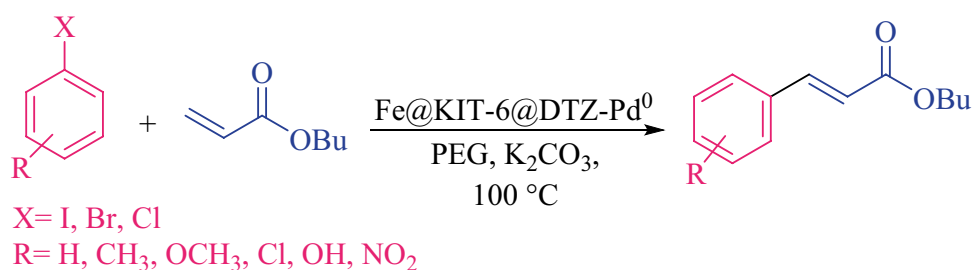
**Suzuki–Miyaura cross-coupling reaction.** To consider more activity of Fe<sub>3</sub>O<sub>4</sub>@SiO<sub>2</sub>@KIT-6@DTZ-Pd<sup>0</sup> as the catalyst, the activity of the described catalyst was studied in the Suzuki cross-coupling reaction. The optimization experiment initiated the reaction of iodobenzene with phenylboronic acid in different conditions as a model substrate. Reaction conditions including base, solvent, temperature, the amount of catalyst were screened and the results are summarized in Table 3. The results demonstrated that the highest efficiency was achieved in Ethanol as the solvent, K<sub>2</sub>CO<sub>3</sub> (2.5 mmol), and was 5 mg of catalyst at 75 °C.

The optimal conditions were applied for the reaction of a wide variety of aryl halides with phenylboronic acid (Scheme 2); the results are presented in Table 4.

**Stille cross-coupling reaction.** Herein in the final part of this research project, Stille cross-coupling reaction of various aryl halides and triphenyl tin chloride was investigated in the presence of Fe<sub>3</sub>O<sub>4</sub>@SiO<sub>2</sub>@KIT-6@DTZ-Pd<sup>0</sup>. The reaction parameters (including solvent, temperature, type, and amount of base as well as the amount of catalyst) were considered for the cross-coupling of iodobenzene and triphenyl tin chloride. As is evident from Table 5 the highest product yield was obtained in PEG as solvent. Also, the highest yield and the

Entry	Solvent	Base	Base (mmol)	Catalyst (mg)	Temperature (°C)	Time (min)	Yield (%) <sup>a</sup>
1	PEG	K <sub>2</sub> CO <sub>3</sub>	3	5	100	35	95
2	DMSO	K <sub>2</sub> CO <sub>3</sub>	3	5	100	35	67
3	DMF	K <sub>2</sub> CO <sub>3</sub>	3	5	100	35	65
4	CH <sub>3</sub> CN	K <sub>2</sub> CO <sub>3</sub>	3	5	Reflux	35	59
5	PEG	KOH	3	5	100	35	53
6	PEG	Na <sub>2</sub> CO <sub>3</sub>	3	5	100	35	76
7	PEG	Li <sub>2</sub> CO <sub>3</sub>	3	5	100	35	61
8	PEG	NaOH	3	5	100	35	45
9	PEG	K <sub>2</sub> CO <sub>3</sub>	3	6	100	35	96
10	PEG	K <sub>2</sub> CO <sub>3</sub>	3	4	100	35	54
11	PEG	K <sub>2</sub> CO <sub>3</sub>	1.5	5	100	35	63
12	PEG	K <sub>2</sub> CO <sub>3</sub>	3	5	120	35	96
13	PEG	K <sub>2</sub> CO <sub>3</sub>	3	5	80	35	65
14	PEG	K <sub>2</sub> CO <sub>3</sub>	3	5	60	35	33

**Table 1.** Optimization conditions of Mizoroki–Heck cross-coupling reaction of iodobenzene and butyl acrylate. Significant values are in bold. <sup>a</sup>Isolated yield.



**Scheme 1.** Mizoroki–Heck cross-coupling reaction.

Entry	X	R	Time (min)	Yield (%) <sup>a</sup>	M.P (°C)	TON	TOF (h <sup>-1</sup> )
1	I	H	35	95	Oil <sup>38</sup>	177.73	304.85
2	I	4-CH <sub>3</sub>	20	92	Oil <sup>38</sup>	172.123	516.88
3	I	4-OCH <sub>3</sub>	15	90	Oil <sup>30</sup>	168.381	673.52
4	Br	4-OCH <sub>3</sub>	40	90	Oil <sup>38</sup>	168.381	252.825
5	Br	4-CH <sub>3</sub>	75	87	Oil <sup>38</sup>	162.768	130.215
6	Br	H	130	85	Oil <sup>38</sup>	159.027	61.164
7	Br	4-Cl	145	89	Oil <sup>39</sup>	166.510	68.92
8	Br	4-NO <sub>2</sub>	180	85	60–61 <sup>38</sup>	159.027	53.009
9	Cl	H	270	79	Oil <sup>31</sup>	147.801	32.844

**Table 2.** Mizoroki–Heck cross-coupling reaction in the presence of a catalytic amount of Fe<sub>3</sub>O<sub>4</sub>@SiO<sub>2</sub>@KIT-6@DTZ-Pd<sup>0</sup>. <sup>a</sup>Isolated yield.

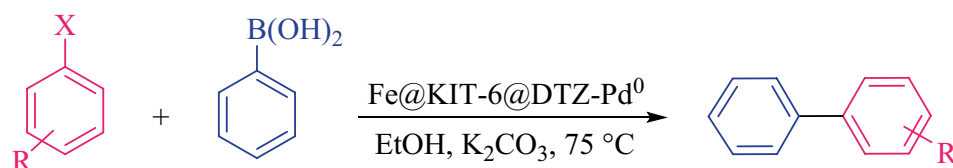
shortest time for mentioned cross-coupling reaction was obtained using K<sub>2</sub>CO<sub>3</sub> as the base, 6 mg of Fe<sub>3</sub>O<sub>4</sub>@SiO<sub>2</sub>@KIT-6@DTZ-Pd<sup>0</sup> at 80 °C.

To spread out the application of described catalyst in Stille reaction; triphenyl tin chloride reacted with a variety of aryl halides (including chloride, bromide, and iodide) under optimal conditions (Scheme 3). The results including yields and reaction times brought in Table 6.

In order to compare the catalytic performance of Fe<sub>3</sub>O<sub>4</sub>@SiO<sub>2</sub>@KIT-6@DTZ-Pd<sup>0</sup> with the previously reported catalysts, the results of coupling of phenylboronic acid with iodobenzene by the previously reported methods are shown in Table 7. In this comparison, various parameters such as reaction time, reaction conditions, and efficiency with other catalysts were compared. In this work, the C–C bond formation reaction is performed in ethanol as a green solvent and this catalyst almost shows a shorter reaction time and higher performance than the other catalysts.

Entry	Solvent	Base	Base (mmol)	Catalyst (mg)	Temperature (°C)	Time (min)	Yield (%) <sup>a</sup>
1	PEG	K <sub>2</sub> CO <sub>3</sub>	2.5	5	75	12	90
2	<b>EtOH</b>	<b>K<sub>2</sub>CO<sub>3</sub></b>	<b>2.5</b>	<b>5</b>	<b>75</b>	<b>12</b>	<b>95</b>
3	DMF	K <sub>2</sub> CO <sub>3</sub>	2.5	5	75	12	48
4	CH <sub>3</sub> CN	K <sub>2</sub> CO <sub>3</sub>	2.5	5	75	12	59
5	EtOH	KOH	2.5	5	75	12	89
6	EtOH	Na <sub>2</sub> CO <sub>3</sub>	2.5	5	75	12	71
7	EtOH	NaOH	2.5	5	75	12	78
8	EtOH	K <sub>2</sub> CO <sub>3</sub>	3	5	75	10	95
9	EtOH	K <sub>2</sub> CO <sub>3</sub>	2	5	75	12	81
10	EtOH	K <sub>2</sub> CO <sub>3</sub>	2.5	7	75	10	93
11	EtOH	K <sub>2</sub> CO <sub>3</sub>	2.5	6	75	12	92
12	EtOH	K <sub>2</sub> CO <sub>3</sub>	2.5	4	75	12	69
13	EtOH	K <sub>2</sub> CO <sub>3</sub>	2.5	5	60	12	76
14	EtOH	K <sub>2</sub> CO <sub>3</sub>	2.5	5	45	12	51

**Table 3.** Optimization of Suzuki–Miyaura cross-coupling reaction of iodobenzene and phenylboronic acid. Significant values are in bold. <sup>a</sup>Isolated yield.



X = I, Br, Cl  
R = H, CH<sub>3</sub>, OCH<sub>3</sub>, Cl, OH, NO<sub>2</sub>

**Scheme 2.** Suzuki–Miyaura cross-coupling reaction.

Entry	X	R	Time (min)	Yield (%) <sup>a</sup>	M.P (°C)	TON	TOF (h <sup>-1</sup> )
1	I	H	12	95	68–69 <sup>40</sup>	177.73	888.65
2	I	4-CH <sub>3</sub>	8	96	46–48 <sup>41</sup>	179.607	1347.39
3	I	4-OCH <sub>3</sub>	6	96	86–87 <sup>42</sup>	179.607	1796.07
4	Br	4-OH	25	96	162–165 <sup>43</sup>	179.607	431.747
5	Br	4-OCH <sub>3</sub>	30	95	88–89 <sup>44</sup>	177.73	355.46
6	Br	4-CH <sub>3</sub>	40	94	45–48 <sup>41</sup>	175.865	264.062
7	Br	3-OCH <sub>3</sub>	40	94	88–90 <sup>31</sup>	175.865	264.062
8	Br	H	55	92	68–70 <sup>45</sup>	172.123	187.907
9	Br	4-Cl	70	92	69–71 <sup>44</sup>	172.123	147.618
10	Br	4-NO <sub>2</sub>	90	92	113–114 <sup>45</sup>	172.123	114.748
11	Cl	H	180	84	67–68 <sup>40</sup>	157.156	52.385

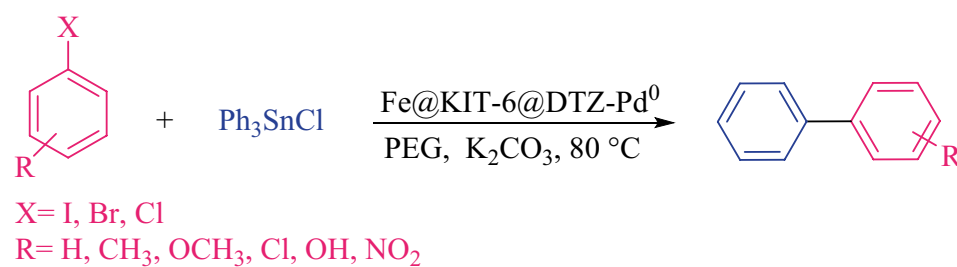
**Table 4.** Suzuki–Miyaura cross-coupling reaction in the presence of a catalytic amount of Fe<sub>3</sub>O<sub>4</sub>@SiO<sub>2</sub>@KIT-6@DTZ-Pd<sup>0</sup>. <sup>a</sup>Isolated yield.

**Reusability of the catalyst.** According to the principles of green chemistry, the recovery of the catalyst at the end of the reaction and its reusability is a highly significant factor. In this aim, Suzuki cross-coupling reaction of iodobenzene and phenylboronic acid was investigated. After each run nanocatalyst was isolated from reaction media by applying a magnet and washed several times with ethanol, then dried and reused for the next experiment. As it can be seen from Fig. 8, the catalyst is recoverable at least up to four runs, with a negligible decrease in its activity.

**Catalyst leaching study.** To perform the hot filtration test, the Suzuki reaction was selected as the model reaction and two types of reactions were performed between iodobenzene and phenylboronic acid under opti-

Entry	Solvent	Base	Base (mmol)	Catalyst (mg)	Temperature (°C)	Time (min)	Yield (%) <sup>a</sup>
<b>1</b>	<b>PEG</b>	<b>K<sub>2</sub>CO<sub>3</sub></b>	<b>3</b>	<b>6</b>	<b>80</b>	<b>35</b>	<b>94</b>
2	DMSO	K <sub>2</sub> CO <sub>3</sub>	3	6	80	35	64
3	DMF	K <sub>2</sub> CO <sub>3</sub>	3	6	80	35	67
4	EtOH	K <sub>2</sub> CO <sub>3</sub>	3	6	Reflux	35	60
5	CH <sub>3</sub> CN	K <sub>2</sub> CO <sub>3</sub>	3	6	80	35	55
6	PEG	KOH	3	6	80	35	75
7	PEG	Na <sub>2</sub> CO <sub>3</sub>	3	6	80	35	71
8	PEG	NaOH	3	6	80	35	68
9	PEG	K <sub>2</sub> CO <sub>3</sub>	1.5	6	80	35	59
10	PEG	K <sub>2</sub> CO <sub>3</sub>	3	7	80	32	94
11	PEG	K <sub>2</sub> CO <sub>3</sub>	3	5	80	35	86
12	K <sub>2</sub> CO <sub>3</sub>	K <sub>2</sub> CO <sub>3</sub>	3	6	100	30	93

**Table 5.** Optimization of Stille cross-coupling reaction of iodobenzene and triphenyl tin chloride. Significant values are in bold. <sup>a</sup>Isolated yield.



**Scheme 3.** Stille reaction by Fe<sub>3</sub>O<sub>4</sub>@SiO<sub>2</sub>@KIT-6@DTZ-Pd<sup>0</sup>.

Entry	X	R	Time (min)	Yield (%) <sup>a</sup>	M.P (°C)	TON	TOF (h <sup>-1</sup> )
1	I	H	35	94	68–69 <sup>44</sup>	175.865	301.655
2	I	4-CH <sub>3</sub>	35	92	43–45 <sup>44</sup>	172.121	288.819
3	I	4-OCH <sub>3</sub>	20	90	85–86 <sup>42</sup>	168.381	505.65
4	Br	4-OH	55	89	162–163 <sup>43</sup>	166.510	181.78
5	Br	4-OCH <sub>3</sub>	60	88	84–86 <sup>42</sup>	164.639	164.639
6	Br	4-CH <sub>3</sub>	70	85	42–43 <sup>43</sup>	159.027	95.454
7	Br	3-OCH <sub>3</sub>	75	87	86–88 <sup>31</sup>	162.768	139.596
8	Br	H	100	90	69–70 <sup>44</sup>	168.381	101.069
9	Br	4-Cl	110	89	69–70 <sup>42</sup>	166.510	90.989
10	Br	4-NO <sub>2</sub>	125	88	112–114 <sup>45</sup>	164.639	79.039
11	Cl	H	240	74	68–69 <sup>44</sup>	138.447	34.611

**Table 6.** Stille cross-coupling reaction in the presence of a catalytic amount of Fe<sub>3</sub>O<sub>4</sub>@SiO<sub>2</sub>@KIT-6@DTZ-Pd<sup>0</sup>. <sup>a</sup>Isolated yield.

mal reaction conditions. In the first reaction, the biphenyl product was obtained after 6 min (half the reaction time) with a yield of 69. Simultaneously in the second reaction, the same reaction was repeated, but at the half-reaction (after 6 min), the catalyst was removed from the reaction mixture by a magnet and the reaction mixture was allowed to run for another 6 min. The reaction efficiency at this stage was 72%. These experiments confirmed that Fe<sub>3</sub>O<sub>4</sub>@SiO<sub>2</sub>@KIT-6@DTZ-Pd<sup>0</sup> was necessary to complete the reaction and that confirmed the leaching of palladium during the reaction didn't occur.

## Conclusions

In this research project, we have introduced a novel magnetic mesoporous material with two unique properties i.e. high porosity and magnetism. These two factors make this nanomaterial an efficient and versatile catalyst. The catalytic activity of Fe<sub>3</sub>O<sub>4</sub>@SiO<sub>2</sub>@KIT-6@DTZ-Pd<sup>0</sup> was examined in the variety of cross-coupling reactions



Entry	Catalyst	Conditions	Time	Yield (%)	References
1	Fe <sub>3</sub> O <sub>4</sub> @SiO <sub>2</sub> -T-Se/Pd (II)	K <sub>2</sub> CO <sub>3</sub> , EtOH: H <sub>2</sub> O, 60 °C	30 min	95	<sup>46</sup>
2	Pd-AcAc-Am-Fe <sub>3</sub> O <sub>4</sub> @SiO <sub>2</sub>	K <sub>2</sub> CO <sub>3</sub> , DMF: H <sub>2</sub> O, 80 °C	1 h	96	<sup>47</sup>
3	Fe <sub>3</sub> O <sub>4</sub> @SiO <sub>2</sub> -APTMS-SAL-Pd	Na <sub>2</sub> CO <sub>3</sub> , EtOH: H <sub>2</sub> O, 75 °C	15 min	98	<sup>48</sup>
4	GO/Fe <sub>3</sub> O <sub>4</sub> /PAMPS/Pd	K <sub>2</sub> CO <sub>3</sub> , EtOH: H <sub>2</sub> O, 80 °C	2 h	100	<sup>49</sup>
5	Pd/Fe <sub>3</sub> O <sub>4</sub> /r-GO	K <sub>2</sub> CO <sub>3</sub> , H <sub>2</sub> O, reflux	15 min	> 99	<sup>50</sup>
6	Pd/chamomile@Fe <sub>3</sub> O <sub>4</sub>	K <sub>2</sub> CO <sub>3</sub> , EtOH: H <sub>2</sub> O, 60 °C	1 h	96	<sup>51</sup>
7	Fe <sub>3</sub> O <sub>4</sub> @MCM-41@Pd-SPATB	K <sub>2</sub> CO <sub>3</sub> , PEG, 80 °C	25 min	94	<sup>52</sup>
8	Fe <sub>3</sub> O <sub>4</sub> @MCM-41-SB-Pd	K <sub>2</sub> CO <sub>3</sub> , DMF, 120 °C	5 min	98	<sup>53</sup>
9	Fe <sub>3</sub> O <sub>4</sub> @SiO <sub>2</sub> @KIT-6@DTZ-Pd <sup>0</sup>	K <sub>2</sub> CO <sub>3</sub> , EtOH, 75 °C	12 min	95	This work

**Table 7.** Comparison of Fe<sub>3</sub>O<sub>4</sub>@SiO<sub>2</sub>@KIT-6@DTZ-Pd<sup>0</sup> with other catalysts for Suzuki–Miyaura reaction using iodobenzene and phenylboronic acid.

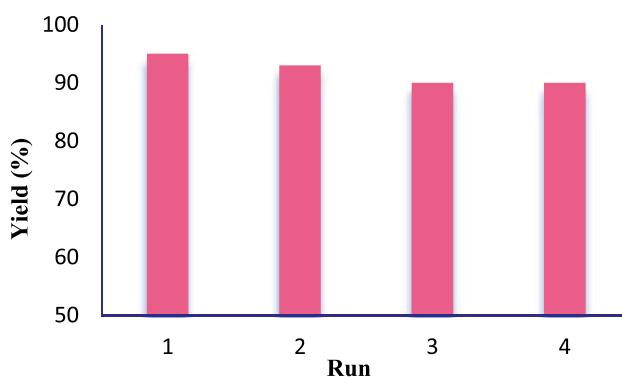


**Figure 8.** Reusability of Fe<sub>3</sub>O<sub>4</sub>@SiO<sub>2</sub>@KIT-6@DTZ-Pd<sup>0</sup> in the synthesis of biphenyl.

including Heck, Suzuki, and Stille reactions. These coupling reactions are performed in environmental-friendly conditions with short reaction times and high efficiency and purity of products.

## Experimental

**Preparation of Fe<sub>3</sub>O<sub>4</sub>@SiO<sub>2</sub>@KIT-6.** For the synthesis of Fe<sub>3</sub>O<sub>4</sub>@SiO<sub>2</sub>@KIT-6, initially, Fe<sub>3</sub>O<sub>4</sub>@SiO<sub>2</sub> nanoparticles were synthesized using the previously reported procedure in the literature<sup>54</sup>. In the next step, P123 (1.25 g), Fe<sub>3</sub>O<sub>4</sub>@SiO<sub>2</sub> (1 g), HCl (37% wt) (2.4 mL), and 1.3 g of *n*-butanol (99.4% wt) were mixed in distilled water (45 mL) and stirred at 35 °C for an hour, then 2.7 g of TEOS was added and the mixture was stirring in the same temperature under nitrogen atmosphere. Finally, the resulting mixture is transmitted into an autoclave and placed in the oven for 24 h at 100 °C. The resulting mixture was washed with 300 mL of ethanol and 20 mL of HCl. Finally, Fe<sub>3</sub>O<sub>4</sub>@SiO<sub>2</sub>@KIT-6 was calcified at 550 °C for 6 h.

**Preparation of Fe<sub>3</sub>O<sub>4</sub>@SiO<sub>2</sub>@KIT-6@DTZ.** In a 100 mL balloon, Fe<sub>3</sub>O<sub>4</sub>@SiO<sub>2</sub>@KIT-6 (1 g) sonicated for 30 min in toluene (25 mL), then, 1.5 mL of 3-chloropropyltriethoxysilane (CPTES) was added and the resulting mixture was stirred for 24 h at 90 °C under nitrogen atmosphere. The obtained solid material was washed with dichloromethane (50 mL). Subsequently, Fe<sub>3</sub>O<sub>4</sub>@SiO<sub>2</sub>@KIT-6@CPTES (1 g) was dispersed in 25 mL of DMF by sonication for 30 min, which was followed by adding 3 mmol of dithizone (diphenylthiocarbazon) and 3.5 mmol triethylamine. The resulting mixture was stirred for 48 h at 100 °C with. The obtained precipitate was then washed several times by organic solvents and dried at room temperature.

**Preparation of Fe<sub>3</sub>O<sub>4</sub>@SiO<sub>2</sub>@KIT-6@DTZ-Pd<sup>0</sup>.** In a 100 mL round-bottom flask Fe<sub>3</sub>O<sub>4</sub>@SiO<sub>2</sub>@KIT-6@DTZ (1 g) dispersed in 50 mL ethanol via sonication for 20 min. Then, 0.5 g of Pd(OAc)<sub>2</sub> was added to the mixture and stirred for 20 h, at reflux conditions under nitrogen atmosphere. Finally, NaBH<sub>4</sub> (0.6 mmol) was added to the reaction mixture and stirred under the same conditions for 2 more hours. Then, the reaction mixture cooled down to room temperature, and magnetic mesoporous material (Fe<sub>3</sub>O<sub>4</sub>@SiO<sub>2</sub>@KIT-6@DTZ-Pd<sup>0</sup>) was isolated by a magnet and washed several times with ethanol.

**General procedure for Mizoroki–Heck cross-coupling reaction.** To perform Heck reaction, in a 5 mL round bottom flask, aryl halide (1 mmol), butyl acrylate (1.2 mmol), 3 mmol of potassium carbonate, and Fe<sub>3</sub>O<sub>4</sub>@SiO<sub>2</sub>@KIT-6@DTZ-Pd<sup>0</sup> (5 mg) were added to 2 mL of PEG and the mixture stirred at 100 °C. The progress of the reaction was followed by TLC. After completion of cross-coupling reaction, 10 mL water was added

and catalyst separated by an external magnet. The corresponding product was extracted by ethyl acetate from a mixture of water and ethyl acetate.

*n-Butyl cinnamate*. mp: Oil (lit.ref Oil);  $^1\text{H NMR}$  (300 MHz,  $\text{CDCl}_3$ ):  $\delta$  7.67–7.72 (d,  $J$  = 7.69, 1H, alkene), 7.52 (d,  $J$  = 7.52, 2H, ArH), 7.39–7.40 (t,  $J$  = 7.39, 2H, ArH), 7.37–7.38 (t,  $J$  = 7.38, 1H, ArH), 6.43–6.48 (d,  $J$  = 4.55, 1H, alkene), 4.22 (t,  $J$  = 4.22, 2H, CH<sub>2</sub>), 1.70 (m,  $J$  = 1.68, 2H, CH<sub>2</sub>), 1.43–1.46 (m,  $J$  = 1.44, 2H, CH<sub>2</sub>), 0.96 (t,  $J$  = 0.97, 3H, CH<sub>3</sub>) ppm (Fig. S1).

**General procedure for Suzuki–Miyaura cross-coupling reaction.** To a 5 mL round bottom flask, aryl halide (1 mmol), phenylboronic acid (1 mmol), potassium carbonate (2.5 mmol), catalyst (5 mg), and 2 mL of ethanol solvent were added. The reaction mixture was stirred for a specified time at 75 °C. After reaction completion, the catalyst was separated using an external magnet and the reaction mixture was transferred to a separating funnel and extracted with ethanol. The extracted organic phase was collected and dried. The obtained product was then spectrally analyzed after purification.

*4-Methyl-1,1'-biphenyl*. mp: 45–48 °C (lit.ref 50–51 °C); TLC (n-hexane);  $^1\text{H NMR}$  (500 MHz, DMSO-*d*<sub>6</sub>)  $\delta$  7.62 (d,  $J$  = 7.63, 2H, ArH), 7.54 (d,  $J$  = 7.55, 2H, ArH), 7.44 (t,  $J$  = 7.44, 2H, ArH), 7.33 (t,  $J$  = 7.33, 1H, ArH), 7.27 (d,  $J$  = 7.26, 2H, ArH), 2.34 (s, 3H, CH<sub>3</sub>) ppm (Fig. S2).

*4-Nitrobiphenyl*. mp: 113–114 °C (lit.ref 103–106 °C); TLC (n-hexane);  $^1\text{H NMR}$  (300 MHz,  $\text{CDCl}_3$ )  $\delta$  8.29–8.30 (d,  $J$  = 8.30, 2H, ArH), 7.72–7.76 (d,  $J$  = 7.74, 2H, ArH), 7.62–7.63 (d,  $J$  = 7.62, 2H, ArH), 7.51 (t,  $J$  = 7.52, 2H, ArH), 7.48 (t, 1H, ArH) ppm (Fig. S3).

**General procedure for Stille cross-coupling reaction.** In a 5 mL round bottom flask, aryl halide (1 mmol), triphenyl tin chloride (0.5 mmol), potassium carbonate (3 mmol), catalyst (6 mg), and 2 mL of PEG solvent were added. The reaction mixture was stirred for a specified time at 80 °C. The reaction progress followed by TLC. After the reaction completion, the catalyst was separated by an external magnetic field, and the mixture was transferred to a separating funnel and extracted with ethyl acetate and water. The obtained organic phase was collected and dried. The obtained product was then spectrally analyzed after purification.

*[1,1'-Biphenyl]-4-ol*. mp: 162–163 °C (lit.ref 161–164 °C); TLC (n-hexane);  $^1\text{H NMR}$  (500 MHz, DMSO-*d*<sub>6</sub>)  $\delta$  9.60 (s, 1H, OH), 7.56 (d,  $J$  = 7.56, 2H, ArH), 7.48 (d,  $J$  = 7.49, 2H, ArH), 7.39 (t,  $J$  = 7.39, 2H, ArH), 7.26 (t,  $J$  = 7.26, 1H, ArH), 6.88 (d,  $J$  = 6.89, 2H, ArH) ppm (Fig. S4).

*4-Chlorobiphenyl*. mp: 69–70 °C (lit.ref 70–72 °C); TLC (n-hexane);  $^1\text{H NMR}$  (500 MHz, DMSO-*d*<sub>6</sub>):  $\delta$  7.68 (d,  $J$  = 7.67, 2H, ArH), 7.66 (d,  $J$  = 7.64, 2H, ArH), 7.51 (d,  $J$  = 7.5, 2H, ArH), 7.46 (t,  $J$  = 7.46, 2H, ArH), 7.38 (t,  $J$  = 7.38, 1H, ArH) ppm (Fig. S5).

Received: 24 August 2021; Accepted: 3 December 2021

Published online: 14 December 2021

## References

- Polarz, S. & Smarsly, B. Nanoporous materials. *J. Nanosci. Nanotechnol.* **2**, 581–612 (2002).
- Selvam, P., Bhatia, S. K. & Sonwane, C. G. Recent advances in processing and characterization of periodic mesoporous MCM-41 silicate molecular sieves. *Ind. Eng. Chem. Res.* **40**, 3237–3261 (2001).
- Li, W. & Zhao, D. An overview of the synthesis of ordered mesoporous materials. *Chem. Commun.* **49**, 943–946 (2013).
- Mohamed, M. G. *et al.* Construction hierarchically mesoporous/microporous materials based on block copolymer and covalent organic framework. *J. Taiwan Inst. Chem. Eng.* **112**, 180–192 (2020).
- Najib, A. S. B. M. *et al.* Active faceted nanoporous ruthenium for electrocatalytic hydrogen evolution. *J. Mater. Chem. A* **8**, 19788–19792 (2020).
- Kumeria, T., Santos, A. & Losic, D. Nanoporous anodic alumina platforms: Engineered surface chemistry and structure for optical sensing applications. *Sensors (Switzerland)* **14**, 11878–11918 (2014).
- Zhang, J. & Li, C. M. Nanoporous metals: Fabrication strategies and advanced electrochemical applications in catalysis, sensing and energy systems. *Chem. Soc. Rev.* **41**, 7016–7031 (2012).
- Yoo, D. *et al.* Porosity control of nanoporous CuO by polymer confinement effect. *Scripta Mater.* **162**, 58–62 (2019).
- Nikoorazm, M. & Ghobadi, M. Cu-SBTU@MCM-41: As an efficient and reusable nanocatalyst for selective oxidation of sulfides an oxidative coupling of thiols. *SILICON* **11**, 983–993 (2019).
- Comini, E. *et al.* Quasi-one dimensional metal oxide semiconductors: Preparation, characterization and application as chemical sensors. *Prog. Mater. Sci.* **54**, 1–67 (2009).
- Savic, S. *et al.* Hard template synthesis of nanomaterials based on mesoporous silica. *Metal. Mater. Eng.* <https://doi.org/10.30544/400> (2018).
- Costa, J. A. S. *et al.* Recent progresses in the adsorption of organic, inorganic, and gas compounds by MCM-41-based mesoporous materials. *Microporous Mesoporous Mater.* **291**, 109698 (2020).
- Kleitzi, F., Choi, S. H. & Ryoo, R. Cubic Ia3d large mesoporous silica: Synthesis and replication to platinum nanowires, carbon nanorods and carbon nanotubes. *Chem. Commun.* **3**, 2136–2137 (2003).
- Pirez, C., Caderon, J. M., Dacquin, J. P., Lee, A. F. & Wilson, K. Tunable KIT-6 mesoporous sulfonic acid catalysts for fatty acid esterification. *ACS Catal.* **2**, 1607–1614 (2012).
- Falahati, M. *et al.* Highly efficient immobilization of beta-lactoglobulin in functionalized mesoporous nanoparticles: A simple and useful approach for enhancement of protein stability. *Biophys. Chem.* **165–166**, 13–20 (2012).

16. He, F., Luo, J. & Liu, S. Novel metal loaded KIT-6 catalysts and their applications in the catalytic combustion of chlorobenzene. *Chem. Eng. J.* **294**, 362–370 (2016).
17. Khabazipour, M., Shariati, S. & Safa, F. SBA and KIT-6 mesoporous silica magnetite nanoparticles: Synthesis and characterization. *Synth. React. Inorg., Met.-Org., Nano-Met. Chem.* **46**, 759–765 (2016).
18. Vinu, A. *et al.* Three-dimensional ultralarge-pore Ia3d mesoporous silica with various pore diameters and their application in biomolecule immobilization. *Chem. Eur. J.* **14**, 11529–11538 (2008).
19. Fischer, C. & Koenig, B. ChemInform Abstract: Palladium- and copper-mediated N-aryl bond formation reactions for the synthesis of biological active compounds. *ChemInform* **42** (2011).
20. Bagherzadeh, M., Hosseini, H. & Salami, R. Polyoxometalate-supported Pd nanoparticles as efficient catalysts for the Mizoroki–Heck cross-coupling reactions in PEG medium. *Appl. Organomet. Chem.* **34**, e5287 (2020).
21. Sarhid, I. *et al.* Plasmonic catalysis for the Suzuki–Miyaura cross-coupling reaction using palladium nanoflowers. *New J. Chem.* **43**, 4349–4355 (2019).
22. Fusini, G. *et al.* Polyvinylpyridine-supported palladium nanoparticles: An efficient catalyst for Suzuki–Miyaura coupling reactions. *Catalysts* **10**, 330 (2020).
23. Yousaf, M., Zahoor, A. F., Akhtar, R., Ahmad, M. & Naheed, S. Development of green methodologies for Heck, Chan–Lam, Stille and Suzuki cross-coupling reactions. *Mol. Divers.* **24**, 821–839 (2020).
24. Chaudhari, K. R., Wadawale, A. P. & Jain, V. K. Isolation of chloro-bridged arylpalladium complexes, [Pd 2Ar 2(μ-Cl) 2(PR 3) 2], in palladium catalyzed C–C cross coupling reaction of triarylbiomuth with arylhalides. *J. Organomet. Chem.* **698**, 15–21 (2012).
25. Le Bras, J. & Muzart, J. Pd-catalyzed intermolecular dehydrogenative heck reactions of five-membered heteroarenes. *Catalysts* **10**, 571 (2020).
26. Ghorbani-Choghamarani, A. & Taherinia, Z. Synthesis, characterization and catalytic application of Bi2S3 microspheres for Suzuki–Miyaura cross-coupling reaction and chemoselective ring opening of epoxides. *Mol. Catal.* **499**, 111283 (2021).
27. Serrano, J. L. & Girase, T. R. Palladacycles as efficient precatalysts for Negishi and Buchwald–Hartwig amination reactions. in *Palladacycles* 175–224 (Elsevier, 2019). <https://doi.org/10.1016/b978-0-12-815505-9.00004-4>
28. Batmani, H., Noroozi Pesyan, N. & Havasi, F. Synthesis and characterization of MCM-41-Biurea-Pd as a heterogeneous nanocatalyst and using its catalytic efficacy in C–C, C–N and C–O coupling reactions. *Appl. Organomet. Chem.* **32**, e4419 (2018).
29. Mohajer, F., Mohammadi Ziarani, G. & Badieli, A. Decorated palladium nanoparticles on mesoporous organosilicate as an efficient catalyst for Sonogashira coupling reaction. *J. Iran. Chem. Soc.* **18**, 589–601 (2021).
30. Kaur, H., Kumar, M. & Bhalla, V. A photocatalytic ensemble HP-T@ Au-Fe<sub>3</sub>O<sub>4</sub>: Synergistic and balanced operation in Kumada and Heck coupling reactions. *Green Chem.* **22**, 8036–8045 (2020).
31. Rahimi, L., Mansoori, Y., Nuri, A., Koochi-Zargar, B. & Esquivel, D. A new Pd (II)-supported catalyst on magnetic SBA-15 for C–C bond formation via the Heck and Hiyama cross-coupling reactions. *Appl. Organomet. Chem.* **35**, e6078 (2021).
32. Sarvestani, M. & Azadi, R. Buchwald–Hartwig amination reaction of aryl halides using heterogeneous catalyst based on Pd nanoparticles decorated on chitosan functionalized graphene oxide. *Appl. Organomet. Chem.* **32**, 1–9 (2018).
33. Jani, M. A. & Bahrami, K. BNPs@Cur-Pd as a versatile and recyclable green nanocatalyst for Suzuki, Heck and Stille coupling reactions. *J. Exp. Nanosci.* **15**, 182–201 (2020).
34. Baran, N. Y., Baran, T., Nasrollahzadeh, M. & Varma, R. S. Pd nanoparticles stabilized on the Schiff base-modified boehmite: Catalytic role in Suzuki coupling reaction and reduction of nitroarenes. *J. Organomet. Chem.* **900**, 120916 (2019).
35. Dabiri, M., Fazli, H., Salarinejad, N. & Movahed, S. K. Pd nanoparticles supported on cubic shaped ZIF-based materials and their catalytic activates in organic reactions. *Mater. Res. Bull.* **133**, 111015 (2021).
36. Toutounchi, S., Shariati, S. & Mahanpoor, K. Synthesis of nano-sized magnetite mesoporous carbon for removal of Reactive Yellow dye from aqueous solutions. *Appl. Organomet. Chem.* **33**, e5046 (2019).
37. Khan, M. *et al.* Miswak mediated green synthesized palladium nanoparticles as effective catalysts for the Suzuki coupling reactions in aqueous media. *J. Saudi Chem. Soc.* **21**, 450–457 (2017).
38. He, L., Jia, C., Zhang, Y. & He, J. Visible light catalyzed step-growth polymerization through Mizoroki–Heck coupling reaction. *Macromol. Rapid Commun.* **41**, 1900640 (2020).
39. Naghipour, A. *et al.* A comparative study of palladium-based coordination compounds with bidentate (N, N, P, P and P, O) ligands; Design, synthesis, X-ray structural, catalytic activity and DFT studies. *Inorg. Chim. Acta* **515**, 120039 (2021).
40. Kempasiddhaiah, M. *et al.* Magnetite tethered mesoionic carbene-palladium (II): An efficient and reusable nanomagnetic catalyst for Suzuki–Miyaura and Mizoroki–Heck cross-coupling reactions in aqueous medium. *Appl. Organomet. Chem.* **33**, e4846 (2019).
41. Soltani, S. S., Taheri-Ledari, R., Farnia, S. M. F., Maleki, A. & Foroumadi, A. Synthesis and characterization of a supported Pd complex on volcanic pumice laminates textured by cellulose for facilitating Suzuki–Miyaura cross-coupling reactions. *RSC Adv.* **10**, 23359–23371 (2020).
42. Maleki, A., Taheri-Ledari, R., Ghalavand, R. & Firouzi-Haji, R. Palladium-decorated o-phenylenediamine-functionalized Fe<sub>3</sub>O<sub>4</sub>/SiO<sub>2</sub> magnetic nanoparticles: A promising solid-state catalytic system used for Suzuki–Miyaura coupling reactions. *J. Phys. Chem. Solids* **136**, 109200 (2020).
43. Nouri, K., Ghassemzadeh, M., Mohsenzadeh, F. & Afsharpour, M. Pd(0) complex of fuberidazole modified magnetic nanoparticles: A novel magnetically retrievable high-performance catalyst for Suzuki and Stille C–C coupling reactions. *Appl. Organomet. Chem.* **34**, 1–15 (2020).
44. Nikoorazm, M., Khanmoradi, M. & Abdi, Z. A highly efficient palladium complex supported on MCM-41 nanocatalyst for Mizoroki–Heck and Suzuki–Miyaura cross-coupling reaction. *J. Iran. Chem. Soc.* **17**, 2577–2585 (2020).
45. Hamid, S. & Mouradzadegan, A. Design and synthesis of supramolecular polymer network equipped with Pd-porphyrin: An efficient and recoverable heterogeneous catalyst for C–C coupling reactions. *Catal. Lett.* **151**, 658–669 (2021).
46. Rangraz, Y., Nemati, F. & Elhampour, A. A novel magnetically recoverable palladium nanocatalyst containing organoselenium ligand for the synthesis of biaryls via Suzuki–Miyaura coupling reaction. *J. Phys. Chem. Solids* **138**, 109251 (2020).
47. Vibhute, S. P., Mhaldar, P. M., Shejwal, R. V. & Pore, D. M. Magnetic nanoparticles-supported palladium catalyzed Suzuki–Miyaura cross coupling. *Tetrahedron Lett.* **61**, 151594 (2020).
48. Amirmahani, N., Mahmoodi, N. O. & Malakootian, M. Pd nanoparticles supported on Fe<sub>3</sub>O<sub>4</sub>@SiO<sub>2</sub>-Schiff base as an efficient magnetically recoverable nanocatalyst for Suzuki–Miyaura coupling reaction. *Res. Chem. Intermed.* <https://doi.org/10.1007/s11164-020-04223-7> (2020).
49. Asadi, S., Sedghi, R. & Heravi, M. M. Pd nanoparticles immobilized on supported magnetic GO @ PAMPS as an auspicious catalyst for Suzuki–Miyaura coupling reaction. *Catal. Lett.* **147**, 2045–2056 (2017).
50. Hoseini, S. J., Heidari, V. & Nasrabadi, H. Magnetic Pd/Fe<sub>3</sub>O<sub>4</sub>/reduced-graphene oxide nanohybrid as an efficient and recoverable catalyst for Suzuki–Miyaura coupling reaction in water. *J. Mol. Catal. A Chem.* **396**, 90–95 (2015).
51. Veisi, H., Zohrabi, A., Ahany, S. & Karmakar, B. Green synthesis of Pd/Fe<sub>3</sub>O<sub>4</sub> nanoparticles using Chamomile extract as highly active and recyclable catalyst for Suzuki coupling reaction. *J. Organomet. Chem.* **951**, 122005 (2021).
52. Nikoorazm, M., Ghorbani, F., Ghorbani-Choghamarani, A. & Erfani, Z. Pd(0)-S-propyl-2-aminobenzothioate immobilized onto functionalized magnetic nanoporous MCM-41 as efficient and recyclable nanocatalyst for the Suzuki, Stille and Heck cross coupling reactions. *Appl. Organomet. Chem.* **32**, 1–13 (2018).

53. Ahmadi, A., Sedaghat, T., Azadi, R. & Motamedi, H. Magnetic mesoporous silica nanocomposite functionalized with palladium Schiff base complex: Synthesis, characterization, catalytic efficacy in the Suzuki–Miyaura reaction and  $\alpha$ -amylase immobilization. *Catal. Lett.* <https://doi.org/10.1007/s10562-019-02913-5> (2019).
54. Shiri, L., Heidari, L. & Kazemi, M. Magnetic Fe<sub>3</sub>O<sub>4</sub> nanoparticles supported imine/Thiophene-nickel (II) complex: A new and highly active heterogeneous catalyst for the synthesis of polyhydroquinolines and 2, 3-dihydroquinazoline-4(1H)-ones. *Appl. Organomet. Chem.* **32**, 1–11 (2018).

### Acknowledgements

This work was supported by the research facilities of Ilam University and Bu-Ali Sina University.

### Author contributions

Zahra Moradi did the experimental works, wrote the manuscript draft and drew the images, schemes and Figures. Arash Ghorbani-Choghamarani supervised the research project and is the corresponding author of the manuscript.

### Competing interests

The authors declare no competing interests.

### Additional information

**Supplementary Information** The online version contains supplementary material available at <https://doi.org/10.1038/s41598-021-03485-4>.

**Correspondence** and requests for materials should be addressed to A.G.-C.

**Reprints and permissions information** is available at [www.nature.com/reprints](http://www.nature.com/reprints).

**Publisher's note** Springer Nature remains neutral with regard to jurisdictional claims in published maps and institutional affiliations.



**Open Access** This article is licensed under a Creative Commons Attribution 4.0 International License, which permits use, sharing, adaptation, distribution and reproduction in any medium or format, as long as you give appropriate credit to the original author(s) and the source, provide a link to the Creative Commons licence, and indicate if changes were made. The images or other third party material in this article are included in the article's Creative Commons licence, unless indicated otherwise in a credit line to the material. If material is not included in the article's Creative Commons licence and your intended use is not permitted by statutory regulation or exceeds the permitted use, you will need to obtain permission directly from the copyright holder. To view a copy of this licence, visit <http://creativecommons.org/licenses/by/4.0/>.

© The Author(s) 2021